Mon. Not. R. Astron. Soc. **000**, 000–000 (0000) Printed 1 February 2008 (MN LATEX style file v1.4)

Newtonian models for black hole–gaseous star close binary systems

Kōji Uryū[1,2] and Yoshiharu Eriguchi[3]
[1] *International Center for Theoretical Physics, Strada Costiera 11, 34100 Trieste, Italy*
[2] *SISSA, Via Beirut 2-4, 34013 Trieste, Italy*
[3] *Department of Earth Science and Astronomy, Graduate School of Arts and Sciences, University of Tokyo, Komaba, Meguro, Tokyo 153-8902, Japan*

arXiv:astro-ph/9808120v1 12 Aug 1998

1 February 2008

ABSTRACT
Circularly orbiting black hole–gaseous star close binary systems are examined by using *numerically exact* stationary configurations in the framework of Newtonian gravity. We have chosen a polytropic star for the fluid component of the binary system and considered two ideal situations: 1) a synchronously rotating star and 2) an irrotationally rotating star. They correspond to a rotating star under the influence of viscosity and to that in the inviscid limit, respectively. By analyzing the stationary sequences of binary systems with small separations, we can discuss the final stages of black hole–gaseous star close binary systems. Our computational results show that the binary systems reach the Roche(–Riemann) limit states or the Roche lobe filling states without suffering from hydrodynamical instability due to tidal force for a large parameter range of the mass ratio and the polytropic index. It is very likely that such stable Roche(–Riemann) limits or Roche lobe filling states survive even under the general relativistic effect. Therefore, at the final stage of the evolution which is caused by the emission of gravitational waves, the Roche overflow will occur instead of merging of a black hole and a star

Key words: binaries:close – black hole physics – hydrodynamics – instabilities – methods: numerical – stars:black hole – stars:neutron – stars:white dwarf – stars: rotation

1 INTRODUCTION

Close binary systems containing a stellar mass ($\sim M_\odot$) black hole (BH hereafter) and a neutron star (NS) or a white dwarf (WD) would emit gravitational waves (GW). As a result, the two component stars approach each other almost adiabatically. At the final stage of such an evolution, binary systems would become sources of various astrophysical phenomena. They are one of the most promising sources of gravitational wave emission, which will be detected by the ground based laser interferometric gravitational wave detectors (LIGO/VIRGO/TAMA/GEO, see e.g. Abramovici et al. 1992 and Cutler et al. 1993). They are also expected to be one of the possible sources of γ–ray bursts (GRB) (e.g. Paczyński 1991).

Because of the GW emission, the orbit of a binary system becomes circular and the separation of two components decreases adiabatically. For the final states of such BH–star systems, we can expect several different possibilities (see e.g. Kidder, Will & Wiseman 1992, Lai, Rasio & Shapiro 1993a, and references therein). One is inspiraling on a dynamical time scale as a result of the tidal or the general relativistic (GR) effect. As is well known, there is an innermost stable circular orbit (ISCO) for a test particle around the BH field such as the Schwarzschild solution. Even if the GR effect is neglected, Newtonian tidal field makes the orbital motion unstable as shown in numerical simulations for binary star systems. Furthermore, the dissipation as a result of the GW emission produces a radial component of the velocity. Consequently the binary system would begin to merge by inspiraling dynamically. In other words, the fluid star would fall on to the black hole on a short dynamical time scale. The other possibility is the Roche overflow, i.e. the mass transfer from the fluid star to the black hole. When the star could approach a state in which the Roche lobe is filled up without suffering from dynamical instability, a certain amount of matter of the star would overflow from its Roche lobe to the black hole or environment. Even after this mass overflow, the star and the black hole may still remain in a stable binary system or at least some amount of matter may orbit around the BH longer than the dynamical time scale (see Kochanek 1992, Bildsten & Cutler 1992, and references therein). These two possibilities are also suggested by recent hydrodynam-

© 0000 RAS

ical simulations for synchronously rotating binary systems (Kluźniak & Lee 1997).

Configurations of such binary systems can be approximated well by quasi-stationary models even just before the merging process or the overflow process starts, because the time scale of the GW emission is much longer than the orbital period (see e.g. Shapiro & Teukolsky 1983). Thus we can discuss final stages of the evolution of binary systems by computing sequences of stationary configurations (see e.g. Lai, Rasio & Shapiro 1993b (LRS1 hereafter) and 1994a (LRS2)). Stationary sequences representing evolutionary tracks can be constructed as follows. It is reasonable to assume that the masses of components are conserved during the evolution and that the equation of state (EOS) and the viscosity of the fluid star are fixed. If the time scale of change due to viscosity is much shorter than that of the evolution due to the GW emission, the spin of the NS is synchronized to the orbital motion. We call a point source and a corotating star a Roche type binary configuration. On the other hand, there is another possibility that the binary configuration can tend to settle into a state in which the fluid star rotates with zero vorticity in the inviscid limit (Kochanek 1992 ; Bildsten & Cutler 1992). We call it an irrotational Roche–Riemann (IRR) binary configuration. These two types of configurations correspond to extended models of ellipsoidal equilibria for binary systems studied by Roche and by Aizenman to more realistic models in which deformation and compressibility of fluid are fully taken into account (see e.g. Chandrasekhar 1969 and Aizenman 1968).

By using such stationary configurations, the final stages of the evolution of binary systems can be discussed. As the separation of two objects decreases, the Roche or the IRR type binary system finally reaches a critical distance. The critical distances for these systems are discussed in LRS1 by using the ellipsoidal approximation for the fluid component. The final fates of the BH-NS systems depend on the type of the critical state which the binary system first approaches. As was stated in their paper, there appear to be three types of critical distances in the framework of Newtonian gravity. These critical states can be found by analyzing stationary sequences by expressing physical quantities as a function of the separation of the centers of the mass of binary components, d_G. The turning point of physical quantities such as $J(d_G)$ or $E(d_G)$ corresponds to the point where some instability sets in, where J and E are the total angular momentum and the total energy, respectively.

For the Roche type binaries, the secular instability will set in at the separation for which functions $J(d_G)$ and $E(d_G)$ reach their turning points which correspond to minima of these functions. At this point, the rotation of a gaseous star will change secularly owing to the viscous effect. The point where the dynamical instability will set in is expected to be located at the smaller separation than that of secular instability. The component stars are thought to coalesce as a result of this dynamical instability at this point. According to LRS1 and the well-organized hydrodynamical simulations of synchronously rotating NS-NS binary systems, differences of values of these two distances are rather small and hence the hydrodynamical instability sets in around the states at the turning points of the curves of the physical quantities (see e.g. Rasio & Shapiro 1992, 1994 ; Shibata, Oohara & Nakamura 1997 ; but see also New & Tohline 1997). We denote the separation at the turning point of $J(d_G)$ or $E(d_G)$ as r_{sec}. For the IRR type binaries, the turning point corresponds to the dynamical instability limit and there is no secular instability limit because the system is not subjected to the influence of the viscosity. We denote the radius at the turning point for the IRR sequences as r_{dyn}. Another critical distance for the BH-NS binary sequence is the Roche(–Riemann) limit where the separation of two components is a minimum or the Roche lobe filling state where the matter fills up its Roche lobe. We denote the corresponding separation as r_R.

According to the results of LRS1 in which the ellipsoidal approximation of the polytropic star has been used, the relation $r_R < r_{dyn}$ is always satisfied for the IRR binary systems. In other words, the IRR binary systems at the Roche–Riemann limit are always dynamically unstable. For the Roche binary systems, the conditions $r_R < r_{sec}$ or $r_R < r_{dyn}$ are satisfied for almost all polytropic indices N and almost all mass ratios M_S/M_{BH} in which realistic values for the BH-NS binary systems are included (see also LRS2 section 2.4).

In this paper, we investigate stationary sequences of the Roche and the IRR binary systems for distances near the critical radii. We obtain *numerically exact* stationary configurations of the binary systems. By using these sequences, we will show that, contrary to the results obtained from the ellipsoidal approximation, there exist dynamically stable Roche and IRR configurations in a wide range of parameters, i.e. r_R appears earlier than r_{sec} or r_{dyn} as the separation decreases. This is because those configurations around the critical radii, in particular at r_R, cannot be expressed well by the ellipsoidal approximation even for fairly stiff equations of state because of a large deformation of the stellar envelope due to compressibility (Uryū & Eriguchi 1998a, Paper I hereafter, 1998b). If the Roche(–Riemann) limit appears for the larger separation than the other hydrodynamical instability limit, the final stage of the evolution of binary systems would be drastically different from the previously suggested scenario. In other words, the Roche lobe overflow or the mass transfer from the star to the black hole is likely to occur instead of unstable plunge of the star to the black hole. We will compute stationary sequences for various polytropic EOS's and mass ratios and reveal the interrelation of critical radii on the sequences. Note that whether such a mass transfer proceeds stably or not should be examined carefully because it could depend crucially on the realistic EOS of the NS and so on.

Concerning the gravitational field, it is still very difficult to take into account the GR effect to such binary systems which contain BHs. As a first step of this kind of research, we only treat Newtonian gravity both for the black hole and for the fluid star. However, we will estimate the GR effect and suggest that there exists a possibility of mass overflow from the star component for realistic values of the parameters of binary systems.

Such systems consisting of a point source and a compressible fluid star have not been discussed yet for fully deformed configurations from the standpoint of stationary structures of binary systems. Therefore our present results will be useful when results in Newtonian or GR hydrodynamical simulations of BH–NS or WD systems will be obtained.

2 SOLVING METHOD FOR STATIONARY CONFIGURATIONS OF BH–NS BINARY SYSTEMS

The solving method of synchronously rotating binary systems has been established by several authors (Hachisu & Eriguchi 1984a, 1984b ; Hachisu 1986). Recently, the method for irrotational binary systems has also been developed by the present authors (Paper I). Since detailed computational methods are described in these papers, we will briefly summarize the assumptions, the formulation of the problem and the computational method below.

2.1 Assumptions

As mentioned in Introduction, we consider binary systems consisting of a point source and a compressible fluid star. We assume the polytropic relation for the EOS of the fluid star:

$$p \,=\, K\rho^{1+1/N} = K\Theta^{N+1}\,, \tag{1}$$

where p, ρ, Θ, N and K are the pressure, the density, the Emden function which is proportional to the enthalpy, the polytropic index and a constant, respectively. The Emden function is used in the actual numerical computations. However note that the Emden function defined here is not normalized as usual ones treated in spherical polytropic stars. From the present knowledge of the neutron matter, the realistic NS's are approximated by polytropes with index $N = 0.5 \sim 1$, (see LRS2 and references therein) and some WD's or low mass main sequence stars are approximated by polytropes with $N \sim 1.5$.

As for the gravitational force, we employ Newtonian gravity. The gravitational potential $\phi = \phi_s + \phi_{BH}$ consists of a contribution from the fluid star itself, ϕ_s, and that from the BH, ϕ_{BH}. The former is expressed in the integral form of the Poisson equation as follows:

$$\phi_s(\mathbf{r}) \,=\, -G\int_V \frac{\rho(\mathbf{r}')}{|\,\mathbf{r}-\mathbf{r}'\,|}d^3\mathbf{r}'\,, \tag{2}$$

where G is the gravitational constant and the integration is performed over the stellar interior V. For the latter potential we assume as follows:

$$\phi_{BH}(\mathbf{r}) = -\frac{GM_{BH}}{R}\ , \tag{3}$$

where M_{BH} is the mass of the black hole and R is the distance from the BH to each fluid element of the star.

Because of dissipation due to the GW emission, we may assume that the binary orbit becomes circular before the coalescence. This assumption breaks down when the hydrodynamical instability or the GR effect produces a radial infall velocity. The radius where the infall velocity cannot be ignored is that of the ISCO. On the other hand, since we neglect all GR effects, we can construct exact circularly orbiting binary configurations even when the star fills the Roche lobe. Using these configurations we can discuss the 'purely' hydrodynamical stability of the system. Furthermore, if the star is not so relativistic, we can assume that the evolution due to the GW emission is adiabatic so that the binary can be regarded in a quasi-stationary state just before the coalescence (Shapiro & Teukolsky 1983). We will discuss the GR effect in a later section.

We can also assume the existence of rotating frames of reference whose angular velocity relative to the inertial frame coincides with the orbital angular velocity of the binary system Ω. In this frame, shapes of binary stars are static. We use this rotating frame in the actual computations.

Concerning the spin state of the fluid component, we consider the following two cases. One is a synchronously rotating state (Roche type). In other words, every fluid element of star is rotating with the same constant angular velocity Ω around the axis of orbital rotation of the binary system. The other is an irrotational state in which the vorticity vanishes everywhere in the fluid in the inertial frame of reference (IRR type).

2.2 Formulation of the problem

We use the spherical coordinates (r, θ, φ) whose origin is located at the geometrical center of the star. The distance from the rotational axis to the origin, d_c, is expressed as

$$d_c \,=\, \frac{R_{\rm in} \,+\, R_{\rm out}}{2}, \tag{4}$$

where $R_{\rm in}$ and $R_{\rm out}$ are distances from the rotational axis to the inner and the outer edges of the star (i.e. the points of the star nearest to the rotational axis and furthest from it), respectively. The star is assumed to be equatorially symmetric. Furthermore we assume symmetry about the plane which is defined by the rotational axis and the geometrical center of the star. Since the formulation must be different for the Roche type configurations and for the irrotational models, we will briefly explain two corresponding formulations.

2.2.1 Basic equations for the Roche type binary systems

For the Roche type binary system, the equation of continuity becomes trivial and the equation of motion is integrated to the following Bernoulli's equation:

$$-\,\frac{1}{2}\,\varpi^2\,\Omega^2 \,+\, K\,(N+1)\,\Theta \,+\, \phi \,=\, C\,, \tag{5}$$

where ϖ is the distance from the rotational axis to the fluid particle and defined by

$$\varpi \,=\, \left\{d_c^2 \,+\, r^2\,\sin^2\theta \,+\, 2\,d_c\,r\,\sin\theta\cos\varphi\right\}^{1/2}\ , \tag{6}$$

and C an integration constant. The Emden function can be obtained from equation (5).

The Green's function $1/|\mathbf{r}-\mathbf{r}'|$ which appears in equation (2) can be expanded as follows:

$$\frac{1}{|\,\mathbf{r}-\mathbf{r}'\,|} \,=\, \sum_{n=0}^{\infty} f_n(r,r')\,P_n(\cos\gamma), \tag{7}$$

where $f_n(r,r')$ is defined as,

$$f_n(r,r') = \begin{cases} \dfrac{1}{r}\left(\dfrac{r'}{r}\right)^n\ , & \text{for} \quad r' \le r\ , \\[2ex] \dfrac{1}{r'}\left(\dfrac{r}{r'}\right)^n\ , & \text{for} \quad r \le r'\ . \end{cases} \tag{8}$$

Here $P_n(\cos\gamma)$ is the Legendre function and γ is the angle between two position vectors $\mathbf{r}$ and $\mathbf{r}'$.

2.2.2 Basic equations for the IRR type binary systems

For the IRR binary system, we will solve for *stationary* structures because the star has non-zero spin even in the rotating frame. Since we assume that the vorticity of the fluid component vanishes in the inertial frame, we can introduce the velocity potential $\Phi(\mathbf{r})$ in the inertial frame as follows:

$$\mathbf{v} = \nabla \Phi \,, \tag{9}$$

where $\mathbf{v}$ is the velocity vector in the inertial frame. The Euler equation of the fluid can be integrated to the generalized Bernoulli's equation as follows in the rotating frame:

$$-\,(\mathbf{\Omega}\times\mathbf{r})\cdot\nabla\Phi \,+\, \frac{1}{2}\,|\,\nabla\Phi\,|^2 \,+\, \int\frac{dp}{\rho} \,+\, \phi \,=\, C \,, \tag{10}$$

where $\mathbf{\Omega}$ is the orbital angular velocity vector of the binary which is identical to the angular velocity vector of the rotating frame relative to the inertial frame. Here we have used the stationarity of the configuration in the rotating frame. We note that the steady velocity $\mathbf{u}$ in the rotating frame is related to $\mathbf{v}$ as follows:

$$\mathbf{u} = \mathbf{v} \,-\, \mathbf{\Omega}\times\mathbf{r} \,. \tag{11}$$

Since we assume configurations are in stationary states, the equation of continuity is expressed by using the velocity potential as follows also in the rotating frame:

$$\nabla^2\Phi \,=\, N(\mathbf{\Omega}\times\mathbf{r} \,-\, \nabla\Phi)\cdot\frac{\nabla\Theta}{\Theta} \,. \tag{12}$$

For the IRR binary systems, the Emden function and the velocity potential are basic variables which can be obtained from equations (10) and (12). The boundary conditions for these two variables are as follows:

$$(\nabla\Phi \,-\, \mathbf{\Omega}\times\mathbf{r})\cdot\mathbf{n} \,=\, 0, \qquad \text{on the stellar surface,} \tag{13}$$

$$\Theta \,=\, 0, \qquad \text{on the stellar surface.} \tag{14}$$

2.3 Numerical scheme

These basic equations are transformed into the surface fitted coordinate system for the IRR binary system as described in Paper I. For the Roche binary system, we use the surface fitted coordinate system for models with polytropic index $0 \le N \le 1$. For polytropes with $1 \le N$, we use the ordinary spherical coordinate system. Stationary configurations are obtained by using the SCF method developed by Ostriker & Mark (1968). The detailed numerical method for the Roche binary system can be found in Hachisu (1986) and that for the IRR binary system in Paper I.

Coordinates are discretized as $(r_i, \theta_j, \varphi_k)$ ($0 \le i \le N_r$, $0 \le j \le N_\theta$ and $0 \le k \le N_\varphi$), where $(N_r, N_\theta, N_\varphi)$ are the numbers of grid points. For the Roche type binary systems, we have chosen $(N_r, N_\theta, N_\varphi) = (12, 8, 16)$ for models in the surface fitted coordinates and $(N_r, N_\theta, N_\varphi) = (32, 16, 32)$ for models in the ordinary spherical coordinates. Although the number of grid points for the surface fitted coordinates is smaller than that of the ordinary spherical coordinates, the surface fitted coordinate system attains higher accuracy and greater robustness. We have computed $N = 1$ models by using both coordinate systems and checked that two results agree very well. For example, differences of critical radii were less that 0.5%. For the IRR type binary systems, since the equations are more complicated than those for the Roche type binary systems, we use $(N_r, N_\theta, N_\varphi) = (16, 12, 24)$ to keep higher accuracy. We also take the number of the terms of the Legendre expansion $0 \le n \le N_l$ in the equation (7) up to $N_l = 10$ for the Roche case with the surface fitted coordinate, and for other models $N_l = 14$. In the HSCF scheme, configurations are solved iteratively by starting from a certain initial guess. We can obtain converged solutions after $15 \sim 40$ iterations for the Roche cases and $40 \sim 90$ iterations for the IRR cases.

3 COMPUTATIONAL RESULTS

The stationary solutions have been computed by fixing the mass ratio M_S/M_{BH} and parameters for the EOS, i.e. N and K, where M_S is the mass of the fluid star. Varying the separation of two components $\tilde{d}$, we can compute a series of stationary solutions. We will call it a stationary sequence. As mentioned above, we have considered synchronously rotating models (Roche type binary systems) and irrotational models (IRR type binary systems). The former can be applied to the evolution of binary systems composed of a viscous fluid star, and the latter to that of an inviscid star.

The normalized separation is defined as

$$\tilde{d} \,=\, \frac{d_c \,+\, d_{BH}}{R_0} \,, \tag{15}$$

where d_{BH} is the distance from the rotational axis to the center of the black hole. The quantity R_0 is defined as

$$R_0 \,=\, \frac{R_{\rm out} \,-\, R_{\rm in}}{2}. \tag{16}$$

We note that the BH is orbiting according to the Keplerian law.

We tabulate several dimensionless quantities for stationary sequences around the critical radii. Dimensionless quantities in those tables are defined as follows:

$$\bar{d}_G \,=\, \frac{d_G}{R_N} \,, \quad \bar{\Omega} \,=\, \frac{\Omega}{(\pi G\bar{\rho}_N)^{1/2}} \,,$$

$$\bar{J} \,=\, \frac{J}{(GM_S^3R_N)^{1/2}} \,, \quad \text{and} \quad \bar{E} \,=\, \frac{T \,+\, W \,+\, U}{GM_S^2/R_N} \,, \tag{17}$$

where R_N is the radius of the spherical polytrope with the same mass M_S and the same polytropic index N. The quantity $\bar{\rho}_N$ is defined as $\bar{\rho}_N \,=\, M/(4\pi R_N^3/3)$. These normalizations are the same as those adopted in LRS's papers. The quantities T, W and U are the total kinematic energy, the total potential energy and the total thermal energy defined as usual (see e.g. Tassoul 1978). The separation between the mass centers of two components d_G is calculated as follows:

$$d_G \,=\, \frac{\int_V x\,\rho\,d^3\mathbf{r}'}{M_S} + d_{BH} \,, \tag{18}$$

where x is defined as $x = d_c + r\sin\theta\cos\varphi$. We also tabulate the quantity $T/|W|$. (Note that T includes both the kinetic energy of orbital motion and that of spin, and hence the definition is different from that of LRS1.) The virial constant VC is also tabulated, which is normalized by the total gravitational potential as,

$$VC \,=\, \frac{|\,2\,T \,+\, W \,+\, 3\,U/N\,|}{|\,W\,|}, \tag{19}$$

Table 1. List of computed models for the Roche binary systems. Characters in parentheses denote how the critical radii along each sequence appear (see text).

M_S/M_{BH}	N									
1.0	0.0 (H)	—	—	0.5 (H)	0.6 (Hc)	0.7 (Hc)	0.8 (R)	—	1.0 (R)	1.5 (R)
0.5	0.0 (H)	—	—	0.5 (H)	0.6 (Hc)	0.7 (M)	0.8 (R)	—	1.0 (R)	1.5 (R)
0.2	0.0 (H)	0.3 (H)	0.4 (H)	0.5 (M)	0.6 (R)	0.7 (R)	0.8 (R)	0.9 (R)	1.0 (R)	1.5 (R)
0.1	0.0 (H)	0.3 (H)	0.4 (H)	0.5 (M)	0.6 (R)	0.7 (R)	0.8 (R)	0.9 (R)	1.0 (R)	1.5 (R)

Table 2. Physical quantities at critical radii for the Roche type binary systems. For normalizations of quantities, see equations (17), (18), (20) and (21). For the models with $N = 0$ and 0.5, the first row corresponds to quantities at r_{sec} and the second row corresponds to those at r_R for each mass ratio. For the models with $N = 1$ and 1.5, quantities at r_R are shown.

M_S/M_{BH}	$\hat{d}$	$\hat{d}_G$	$\bar{\Omega}$	$\bar{J}$	$\bar{E}$	$\bar{R}$
			$N = 0$			
1.0	1.945	2.418	3.138(-1)	1.391	-7.377(-1)	9.989(-1)
	1.587	2.316	3.413(-1)	1.412	-7.315(-1)	9.989(-1)
0.5	1.837	2.450	3.079(-1)	2.353	-8.511(-1)	9.989(-1)
	1.595	2.407	3.194(-1)	2.372	-8.461(-1)	9.989(-1)
0.2	1.761	2.486	2.997(-1)	4.552	-1.115	9.989(-1)
	1.596	2.468	3.046(-1)	4.569	-1.111	9.989(-1)
0.1	1.709	2.492	2.974(-1)	7.334	-1.460	9.989(-1)
	1.619	2.482	2.998(-1)	7.343	-1.457	9.989(-1)
			$N = 0.5$			
1.0	1.746	2.267	3.453(-1)	1.334	-7.065(-1)	1.023
	1.587	2.238	3.534(-1)	1.336	-7.058(-1)	1.026
0.5	1.699	2.328	3.311(-1)	2.268	-8.266(-1)	1.025
	1.629	2.320	3.333(-1)	2.269	-8.264(-1)	1.026
0.2	1.623	2.368	3.215(-1)	4.408	-1.105	1.028
	1.596	2.367	3.216(-1)	4.409	-1.105	1.029
0.1	1.574	2.372	3.194(-1)	7.115	-1.468	1.031
	1.574	2.372	3.194(-1)	7.115	-1.468	1.031
			$N = 1.0$			
1.0	1.667	2.207	3.562(-1)	1.286	-6.616(-1)	1.030
0.5	1.664	2.281	3.382(-1)	2.203	-7.860(-1)	1.030
0.2	1.706	2.327	3.272(-1)	4.312	-1.072	1.032
0.1	1.664	2.327	3.269(-1)	6.979	-1.446	1.035
			$N = 1.5$			
1.0	1.667	2.201	3.557(-1)	1.255	-5.963(-1)	1.040
0.5	1.733	2.278	3.373(-1)	2.170	-7.211(-1)	1.039
0.2	1.761	2.322	3.274(-1)	4.272	-1.009	1.040
0.1	1.709	2.317	3.282(-1)	6.926	-1.386	1.044

where the term U/N vanishes for models with $N = 0$. We also show values of the averaged radius $\bar{R}$ defined as follows:

$$\bar{R} = \left(\frac{3\,V}{4\,\pi\,R_N^3}\right)^{\frac{1}{3}} = \left[\frac{1}{4\,\pi\,R_N^3}\int_0^{\pi}\sin\theta\,d\theta\int_0^{2\pi}d\varphi\,R^3(\theta,\varphi)\right]^{\frac{1}{3}}. \quad (20)$$

Generally, this quantity increases as the separation decreases. It implies that the volume of the gaseous star always increases and, accordingly, that the central density decreases as the two components approach during the evolution. In some tables, we also show quantities $\hat{d}$ and $\hat{d}_G$ which are defined as follows:

$$\hat{d} = \frac{d}{R_N(1+M_{BH}/M_S)^{1/3}}$$

$$\hat{d}_G = \frac{d_G}{R_N(1+M_{BH}/M_S)^{1/3}}. \quad (21)$$

d behaves as $d \propto (M_S/M_{BH})^{-1/3}$ for $M_S/M_{BH} \to 0$ limit since the binary system tends to Keplerian, which is the reason of this normalization (see LRS1). Finally, for later discussions, we write down the quadrupole formula for the gravitational radiation emission here. In the rotating frame of reference, the quadrupole moment tensors are defined as

$$I_{ij}^{(rot)} = \rho\int_V (x_i x_j - \delta_{ij}\frac{|\,\mathbf{x}\,|^2}{3})dV, \quad (22)$$

where $i, j = 1, 2, 3$ correspond to the x, y, z-component of the Cartesian coordinates, respectively. By taking the symmetry of the system into account, the quadrupole formula for the angular momentum dissipation rate is written as follows:

$$\frac{dJ}{dt} = -\frac{32\,G}{5\,c^5}\,\Omega^5\,(I_{11}^{(rot)} - I_{22}^{(rot)})^2\,, \tag{23}$$

where c is the speed of light. Derivation of this formula is shown in the book of Misner, Thorne & Wheeler (1970) (see also Eriguchi, Futamase & Hachisu 1990). This angular momentum dissipation rate is related to the energy dissipation rate as follows:

$$\frac{dE}{dt} = \Omega\frac{dJ}{dt} \tag{24}$$

3.1 Results for the Roche type binary systems

3.1.1 Critical radii for the Roche type binary configurations

As mentioned in Introduction, we can discuss the critical radii of binary systems by using the stationary sequences. One can find a comprehensive discussion on these critical radii in LRS's papers in which the ellipsoidal approximation is used (see for example Lai, Rasio & Shapiro 1993a, 1994b).

According to LRS, three different types of critical radii can be identified by examining the behavior of $J(d_G)$ or $E(d_G)$ for the Roche type sequences. The turning point of the $J(d_G)$ or $E(d_G)$ curve corresponds to the point where the secular instability sets in. We denote this separation as r_{sec}. Since the assumption of the synchronous rotation implies that the viscosity of neutron matter is strong enough, viscosity can change the flow field of the fluid star and the star secularly evolves to a configuration with a lower energy even when the system is in a configuration at the turning point of the energy curve. However, we also note that the evolutionary time scale due to the GW emission is almost comparable to the dynamical time scale at the configuration corresponding to the turning point of the energy curve.

There is another critical radius on the sequence where the dynamical instability sets in, i.e. $d_G = r_{dyn}$. To determine r_{dyn}, it is necessary to compute non-synchronously rotating configurations (see LRS1). However, it is difficult to construct such non-synchronously rotating configurations with generic flows (see for e.g. Uryū & Eriguchi 1996, and references therein). According to the ellipsoidal approximation of LRS and the dynamical simulations for the *NS-NS* binary systems (Rasio & Shapiro 1992, 1994 ; Shibata, Oohara & Nakamura 1997 ; Oohara, Nakamura & Shibata 1997 ; Ruffert, Rampp & Janka 1997 ; New & Tohline 1997), r_{dyn} is smaller than that of the secular instability limit, $r_{dyn} < r_{sec}$, and these two radii are very close. For these kinds of *NS–NS* binary systems, they showed that the instability of orbital motion begins around these radii. Since we can expect that the situation is similar for binary systems of a point source and a fluid star, we only discuss r_{sec} hereafter and regard it as the radius where the instability of orbital motion sets in. We also refer to this instability, associated with inspiraling motions, as the hydrodynamical instability in this paper. The origin of this instability is purely a Newtonian tidal effect for the fluid component.

The other critical radius is the Roche limit r_R which

Figure 1. Function $\bar{J}(\bar{d}_G)$ of the Roche sequences for several mass ratios M_S/M_{BH} and polytropic indices N. (a) $M_S/M_{BH} = 1.0$ and $N = 0.5$–0.8. (b) $M_S/M_{BH} = 0.5$ and $N = 0.5$–0.8. (c) $M_S/M_{BH} = 0.2$ and $N = 0.3$–1.0. (d) $M_S/M_{BH} = 0.1$ and $N = 0.3$–1.0. Each curve corresponds to a different polytropic index N. The difference of N between two adjacent curves is 0.1. The upper curve corresponds to the smaller value of N.

corresponds to the smallest separation of the stars along the sequences or the Roche lobe filling states. To determine this limit, we need to compute sequences by changing the parameter $\tilde{d}$ to smaller values until the inner edge of the fluid star forms a cusp. The configuration with such a cusp can be identified as the Roche lobe filling state. The smallest value of d_G is the Roche limit $r_R = d_G$ of the sequence. It should be noted that it is possible for r_R to appear at a larger separation than r_{dyn} or r_{sec} or both and hence the critical radius r_{dyn} or r_{sec} disappears. In this case, by considering equation (23), the evolutionary time scale due to the GW emission does not become zero. Therefore the GW emission would not drive a significant radial velocity. If the GR effect is also negligible, the infall velocity would be a moderate value even at r_R. Consequently, tidal stripping of the fluid component star or tidal disruption without the instability of orbital motion could be expected to occur.

3.1.2 Stationary sequences of the Roche type binary systems

In Table 1, we tabulate model parameters chosen for the Roche type binary systems. They are the mass ratio M_S/M_{BH} and the polytropic index N. We have computed models with $0.1 \lesssim M_S/M_{BH} \lesssim 1$ and $0 \lesssim N \lesssim 1.5$. In Figure 1(a)–(d), we show $\bar{J}(\bar{d}_G)$ for sequences with $M_S/M_{BH} = 1$, 0.5, 0.2 and 0.1, respectively, with several polytropic indices N whose values are $0 < N < 1$. Our results show important differences from those of LRS1. In their results the secular instability limit r_{sec} always appears for any mass ratio and any polytropic index and always satisfies the relation $r_{sec} > r_R$. It can be seen that the turning point of the $\bar{J}(\bar{d}_G)$ curve (i.e. r_{sec}) disappears for $N \sim 0.8$, 0.7, 0.5 and 0.5 with the mass ratio $M_S/M_{BH} = 1$, 0.5, 0.2 and 0.1, respectively.

In Table 1, we roughly classify the sequences by considering the appearance of critical radii along the curves of $J(d_G)$. Three capital letters H, R and M are used as follows:

(i) H denotes that the sequence has a turning point.

(ii) R denotes that the sequence does not have a turning point but directly reaches a state with the smallest separation.

(iii) M denotes that the sequence has a turning point which almost coincides with a state with the smallest separation.

As mentioned before, we have computed sequences by varying $\tilde{d}$ until the cusp is formed at the inner edge of the fluid star. For the H type sequences, some models at r_R have cusps and others do not have cusps. A character c will be used for the models with cusps at r_R. For the R type sequences, the separations of the terminal configurations which fill up the Roche lobe should be the smallest. However, as can be seen in Figure 1(a)–(d), the total angular momentum of the configuration with the cusp, i.e. the left end point of the curves $J(d_G)$, slightly shows an irregular behaviour on the sequence in some cases. This may be because it is relatively difficult to maintain the same accuracy for those 'singular' configurations with cusps as well as for the others. Since such irregular behaviour is very small, we can determine whether the sequence has a turning point or not from these figures. For example, the difference between

Figure 2. Plots of critical radii r_{sec} and r_R for the Roche sequences as a function of the mass ratio M_S/M_{BH}. In panels (a)–(c), present results and those of LRS1 are shown for the polytropic indices $N = 0$, 1.0 and 1.5, respectively. Each curve corresponds to a different critical radius as follows: present result for r_{sec} (dash dotted line), present result for r_R (solid line), result of LRS1 for r_{sec} (short dashed line) and result of LRS1 for r_R (long dashed line). In the panel (d), present results for several polytropic indices $N = 0, 0.5, 1.0$ and 1.5 are drawn. Dash dotted line: r_{sec} for $N = 0$. Solid line: r_R for $N = 0$. Short dashed line: r_{sec} for $N = 0.5$. Long dashed line: r_R for $N = 0.5$. Dotted line: r_R for $N = 1$. Dashed line: r_R for $N = 1.5$.

Table 3. List of computed models for the IRR binary systems. Characters in parentheses denote how the critical radii along each sequence appear (see text).

M_S/M_{BH}	N							
1.0	0.0 (H)	—	—	—	0.5 (Hc)	0.6 (M)	0.7 (R)	1.0 (R)
0.5	0.0 (H)	—	—	—	0.5 (Hc)	0.6 (R)	0.7 (R)	1.0 (R)
0.2	0.0 (H)	—	0.3 (Hc)	0.4 (M)	0.5 (R)	—	—	1.0 (R)
0.1	0.0 (H)	0.2(Hc)	0.3 (M)	0.4 (R)	0.5 (R)	—	—	1.0 (R)

Table 4. Same as Table 2 but for IRR type binary systems. For models with $N = 0$ and $M_S/M_{BH} = 1.0$ and 0.5 of 0.5, the first row corresponds to quantities at r_{sec} and the second row corresponds to those at r_R for each mass ratio. For models with $N = 1$ and 1.5 and $M_S/M_{BH} = 0.2$ and 0.1 of 0.5, quantities at r_R are shown.

M_S/M_{BH}	$\hat{d}$	$\hat{d}_G$	$\bar{\Omega}$	$\bar{J}$	$\bar{E}$	$\bar{R}$
			$N = 0$			
1.0	1.905	2.415	3.152(-1)	1.271	-7.567(-1)	9.994(-1)
	1.627	2.362	3.301(-1)	1.287	-7.506(-1)	9.994(-1)
0.5	1.837	2.483	3.018(-1)	2.244	-8.678(-1)	9.994(-1)
	1.664	2.450	3.101(-1)	2.259	-8.619(-1)	9.994(-1)
0.2	1.761	2.518	2.944(-1)	4.460	-1.126	9.994(-1)
	1.651	2.509	2.969(-1)	4.470	-1.123	9.994(-1)
0.1	1.709	2.527	2.916(-1)	7.258	-1.466	9.994(-1)
	1.619	2.523	2.929(-1)	7.268	-1.463	9.994(-1)
			$N = 0.5$			
1.0	1.667	2.256	3.479(-1)	1.223	-7.240(-1)	1.010
	1.627	2.255	3.484(-1)	1.223	-7.239(-1)	1.010
0.5	1.699	2.336	3.291(-1)	2.162	-8.426(-1)	1.011
	1.664	2.335	3.295(-1)	2.162	-8.426(-1)	1.012
0.2	1.651	2.383	3.184(-1)	4.302	-1.121	1.014
0.1	1.641	2.390	3.160(-1)	7.009	-1.484	1.015
			$N = 1.0$			
1.0	1.706	2.205	3.560(-1)	1.189	-6.780(-1)	1.005
0.5	1.733	2.282	3.378(-1)	2.109	-8.012(-1)	1.008
0.2	1.761	2.328	3.273(-1)	4.214	-1.088	1.010
0.1	1.754	2.337	3.250(-1)	6.887	-1.460	1.012

d_G of a configuration with a cusp and r_R is less than 0.2% for every sequence.

According to the discussion in the previous section, the hydrodynamical instability is expected to occur for all models of (i), and the mass overflow is expected to occur prior to the orbital instability for models of (ii). Since the realistic NS is thought to be approximated by the polytropic EOS with $N \sim 0.5 - 1.0$ (see e.g. Shapiro & Teukolsky 1983) and the WD or the low mass main sequence stars with $N \sim 1.5$, most of realistic situations of the BH–star binary systems correspond to the case (ii).

We tabulate several physical quantities at critical radii, r_{sec} and r_R in Table 2. In Figure 2, we plot these critical radii against the mass ratio. In panels (a)–(c), we compare our results with those of the ellipsoidal approximation tabulated in LRS1 for $N = 0$, 1.0 and 1.5. For $N = 0$, the differences of the values of critical radii are more or less 5% and stationary sequences behave qualitatively similarly for both results. They can be classified to the H type (see Uryū & Eriguchi 1998c). On the other hand, for larger N the quantitative difference becomes larger. It becomes roughly 10% for polytropes with $N = 1$ and 15% for models with $N = 1.5$. Moreover, the turning points disappear on the stationary sequences. In Figure 2(d), we plot our results for polytropes with $N = 0$, 0.5, 1.0 and 1.5. From this figure, it can be clearly shown that the secular instability limit vanishes for larger polytropic indices and for larger mass ratios as mentioned before.

3.2 Results for the IRR type binary systems

3.2.1 Critical radii for the IRR type binary systems

The stationary sequence of the IRR type binary system can be regarded as that composed of an inviscid fluid star. The circulation of each fluid element is conserved under the dissipation due to the GW emission (Miller 1974). Therefore, there is no secular instability limit on the IRR sequence but there are two different types of critical radii on it. The radius at the turning point of the $J(d_G)$ or $E(d_G)$ curve is denoted as r_{dyn}. The other critical radius is the Roche-Riemann limit r_R. The determination of the Roche-Riemann limit is the same as the case of the Roche binary systems. As discussed

in LRS1 the dynamical instability will set in around r_{dyn}. On the other hand, if the r_R is larger than r_{dyn}, i.e. r_{dyn} disappears on the IRR sequence, the dynamical instability would not occur for binary systems during the evolution but the mass overflow would be expected to begin at r_R.

3.2.2 Stationary sequences of the IRR type binary systems

In Table 3, we tabulate model parameters chosen for the IRR type binary systems. The IRR configurations correspond to the inviscid limit of fluid stars which can be applied for the BH–NS systems, because the viscosity is strong enough to synchronize the rotation only for WD or lower main sequence stars. Therefore we have computed polytropes with indices $0 \leq N \leq 1$, which are appropriate for the neutron matter.

In Figure 3(a)–(d), we show the quantity $\bar{J}(\bar{d}_G)$ for sequences with $M_S/M_{BH} = 1$, 0.5, 0.2 and 0.1, respectively. The dynamical instability limit r_{dyn} for each mass ratio sequence disappears for fairly stiff EOS. We can see that the $\bar{J}(\bar{d}_G)$ curves do not extend to the turning points for sequences with $N \sim 0.6$, 0.5, 0.4 and 0.3 for $M_S/M_{BH} = 1$, 0.5, 0.2 and 0.1, respectively. Similar to the Roche binary systems, we can roughly classify those sequences for the IRR binary systems in Table 3 by considering the critical radii. We will use three capital letters H, R and M as before. For the IRR binary systems, the terminal configuration of the R-type sequences always has a cusp. As mentioned before, the hydrodynamical instability would probably occur for the H-type sequences and Roche overflow would be expected for the R-type sequences. From our results, the possibility of Roche overflow survives even for realistic ranges of M_S/M_{BH} and N if the GR effect is neglected.

In Table 4, we tabulate several physical quantities at the critical radii, r_{dyn} and r_R. In Figure 4, we plot these critical radii against the mass ratio. In panels (a) and (b), we compare our results with those of the ellipsoidal approximation tabulated in LRS1 for polytropes with $N = 0$ and 1.0. For $N = 0$ polytropes, the results are the same as those of Uryū & Eriguchi (1998c). On the other hand, the difference amounts to 10–15% for polytropes with $N = 1$. In Figure 2(c), we show our results for polytropes with $N = 0, 0.5$ and 1.0. The dynamical instability limit disappears for the models with larger polytropic indices and with larger mass ratios as mentioned before.

3.3 Configurations of the Roche type and the IRR type binary systems around the critical radii

As shown in previous subsections, we have found that the locations of critical radii, in particular that of r_R, are quite different from those computed from the ellipsoidal approximation (LRS1). Moreover, there is a possibility that the fluid star reaches the Roche(–Riemann) limit without suffering from hydrodynamical instability because the critical radius such as r_{sec} or r_{dyn} disappears on the stationary sequences for rather stiff EOS. The reason for this difference of r_R can be explained by considering the large deformation of the stellar envelope due to compressibility of the stellar matter as follows (see also Paper I): the deformation of the envelope due to the tidal force becomes large, and, in particular, that around the inner parts near the BH becomes

Figure 3. Same as Fig. 1 but for the IRR sequences. (a) $M_S/M_{BH} = 1.0$ and $N = 0.5$–0.7. (b) $M_S/M_{BH} = 0.5$ and $N = 0.5$–0.7. (c) $M_S/M_{BH} = 0.2$ and $N = 0.3$–0.5. (d) $M_S/M_{BH} = 0.1$ and $N = 0.2$–0.5.

Figure 4. Plots of critical radii r_{dyn} and r_R for the IRR sequences as a function of the mass ratio M_S/M_{BH}. In panels (a) and (b), present results and those of LRS1 are shown for the polytropic indices $N = 0$ and 1.0, respectively. Each curve corresponds to a different critical radius as follows: present result for r_{dyn} (dash dotted line), present result for r_R (solid line), result of LRS1 for r_{dyn} (short dashed line) and result of LRS1 for r_R (long dashed line). In the panel (c), present results for several polytropic indices $N = 0, 0.5$ and 1.0 are drawn. Dash dotted line: r_{dyn} for $N = 0$. Solid line: r_R for $N = 0$. Short dashed line: r_{dyn} for $N = 0.5$. Long dashed line: r_R for $N = 0.5$. Dotted line: r_R for $N = 1$.

larger than that of other parts. Because of this significant deformation of the envelope, a cusp is formed at the inner edge and hence the sequence is terminated at a larger separation $d_G = r_R$ than that for the ellipsoidal approximation. Therefore the difference between our results and those of LRS1 for the critical radii becomes significant. In Figures 5 and 6, we show configurations of the fluid components for the Roche type and the IRR type binary systems, respectively.

From panels (a)-(c) of these figures, we can clearly see the difference of the shape in the two cases : the Roche

Figure 5. Distributions of physical quantities for the Roche binary system with $M_S/M_{BH} = 0.1$ and $N = 0.5$ polytrope at the Roche limit r_R. $\tilde{X}\tilde{Y}\tilde{Z}$–coordinates are the Cartesian coordinates where $\tilde{X}$ axis intersects the inner and the outer edges of the star and the rotational center. $\tilde{X}$–$\tilde{Y}$ plane is the equatorial plane. The $\tilde{Z}$ axis is parallel to the rotational axis. The origin of $\tilde{X}\tilde{Y}\tilde{Z}$–coordinates is at the geometrical center of the star and the coordinate is normalized by equation(16). (a) Contours of the density in the equatorial $\tilde{X}$–$\tilde{Y}$ plane. (b) Contours of the density in the meridional $\tilde{X}$–$\tilde{Z}$ plane. (c) Contours of the density in the meridional $\tilde{Y}$–$\tilde{Z}$ plane. The difference between two subsequent contours for each quantity is 1/10 of the difference between the maximum value and the minimum value.

Figure 6. Distributions of physical quantities for the IRR binary system with $M_S/M_{BH} = 0.1$ and $N = 0.5$ polytrope at the Roche-Riemann limit r_R. (a) Contours of the density in the equatorial $\tilde{X}$–$\tilde{Y}$ plane. (b) Contours of the density in the meridional $\tilde{X}$–$\tilde{Z}$ plane. (c) Contours of the density in the meridional $\tilde{Y}$–$\tilde{Z}$ plane. (d) Contours of the velocity potential in the equatorial $\tilde{X}$–$\tilde{Y}$ plane. (e) Contours of the velocity potential in the plane with $\varphi = \pi/16$ and $\varphi = 17\pi/16$. (f) Contours of the velocity potential in the meridional $\tilde{X}$–$\tilde{Z}$ plane. Conventions are the same as Figure 5.

Table 5. Physical quantities for stationary sequences of the Roche binary systems.

$\tilde{d}$	$\bar{d}_G$	$\bar{\Omega}$	$\bar{J}$	$\bar{E}$	$T/\|W\|$	VC	$\bar{R}$
			$M_S/M_{BH} = 1$ and $N = 0.5$				
2.4	2.942	3.286(-1)	1.337	-7.056(-1)	1.893(-1)	3.163(-2)	1.020
2.3	2.894	3.376(-1)	1.335	-7.063(-1)	1.932(-1)	3.130(-2)	1.021
2.2	2.856	3.453(-1)	1.334	-7.065(-1)	1.968(-1)	3.104(-2)	1.023
2.1	2.830	3.510(-1)	1.335	-7.063(-1)	1.996(-1)	3.092(-2)	1.025
2.05	2.823	3.527(-1)	1.335	-7.060(-1)	2.006(-1)	3.096(-2)	1.025
2.0	2.820	3.534(-1)	1.336	-7.058(-1)	2.011(-1)	3.109(-2)	1.026
1.97	2.821	3.532(-1)	1.336	-7.058(-1)	2.010(-1)	3.122(-2)	1.026
			$M_S/M_{BH} = 1$ and $N = 1.0$				
2.6	3.004	3.156(-1)	1.312	-6.539(-1)	1.672(-1)	3.333(-3)	1.019
2.5	2.942	3.260(-1)	1.304	-6.562(-1)	1.708(-1)	3.104(-3)	1.022
2.4	2.887	3.357(-1)	1.298	-6.581(-1)	1.741(-1)	3.335(-3)	1.024
2.3	2.840	3.445(-1)	1.292	-6.598(-1)	1.771(-1)	3.323(-3)	1.026
2.2	2.802	3.518(-1)	1.288	-6.609(-1)	1.798(-1)	3.415(-3)	1.029
2.1	2.780	3.562(-1)	1.286	-6.616(-1)	1.814(-1)	3.418(-3)	1.030
			$M_S/M_{BH} = 1$ and $N = 1.5$				
2.5	2.926	3.275(-1)	1.278	-5.895(-1)	1.535(-1)	1.358(-3)	1.030
2.4	2.871	3.371(-1)	1.270	-5.919(-1)	1.564(-1)	1.332(-3)	1.033
2.3	2.825	3.456(-1)	1.263	-5.940(-1)	1.589(-1)	1.414(-3)	1.036
2.2	2.790	3.522(-1)	1.258	-5.955(-1)	1.608(-1)	1.466(-3)	1.039
2.1	2.773	3.557(-1)	1.255	-5.963(-1)	1.619(-1)	1.536(-3)	1.040
			$M_S/M_{BH} = 0.1$ and $N = 0.5$				
4.0	2.495	3.097(-1)	7.154	-1.458	3.802(-1)	1.311(-2)	1.025
3.9	2.480	3.128(-1)	7.139	-1.462	3.815(-1)	1.310(-2)	1.027
3.8	2.467	3.155(-1)	7.127	-1.465	3.828(-1)	1.313(-2)	1.028
3.7	2.457	3.176(-1)	7.119	-1.467	3.838(-1)	1.320(-2)	1.029
3.6	2.451	3.189(-1)	7.115	-1.468	3.846(-1)	1.336(-2)	1.030
3.5	2.449	3.194(-1)	7.115	-1.468	3.850(-1)	1.363(-2)	1.031
			$M_S/M_{BH} = 0.1$ and $N = 1.0$				
4.0	2.435	3.198(-1)	7.018	-1.435	3.680(-1)	2.258(-3)	1.033
3.9	2.421	3.228(-1)	7.001	-1.440	3.690(-1)	2.246(-3)	1.034
3.8	2.410	3.251(-1)	6.988	-1.444	3.697(-1)	2.242(-3)	1.036
3.7	2.404	3.264(-1)	6.980	-1.446	3.702(-1)	2.260(-3)	1.037
3.6	2.404	3.262(-1)	6.981	-1.446	3.701(-1)	2.252(-3)	1.037
			$M_S/M_{BH} = 0.1$ and $N = 1.5$				
4.3	2.469	3.127(-1)	7.029	-1.358	3.502(-1)	6.646(-4)	1.035
4.2	2.448	3.169(-1)	7.001	-1.365	3.515(-1)	6.709(-4)	1.037
4.1	2.428	3.207(-1)	6.975	-1.372	3.526(-1)	6.937(-4)	1.039
4.0	2.412	3.239(-1)	6.954	-1.378	3.535(-1)	6.947(-4)	1.041
3.9	2.399	3.265(-1)	6.937	-1.383	3.543(-1)	7.055(-4)	1.043
3.8	2.392	3.282(-1)	6.926	-1.386	3.547(-1)	7.292(-4)	1.044

type is oblate and the IRR type is prolate, which is the same as the incompressible case. Finally selected sequences of the Roche type and the IRR type binary systems near the critical points are tabulated in Tables 5 and 6.

4 DISCUSSION AND CONCLUSIONS

4.1 General relativistic effect and the possibility of mass transfer

So far, we have neglected the GR effect in order to focus on the hydrodynamical effect caused by the Newtonian tidal gravitational field. For the realistic BH–star binary systems, the GR effect plays an essential role for the stability of the binary system when the star is sufficiently compact. Kidder, Will & Wiseman (1992) developed a method to compute the radius of ISCO, r_{GR}, by taking the GR effect into consideration to some extent. They treated a system consisting of two point masses including the post-Newtonian effect up to $(v/c)^4$ order and also incorporated the effect of the Schwarzschild geometry exactly. Lai, Rasio & Shapiro proposed a fitting formula for their results in LRS2 as follows:

$$r_{GR} \simeq \frac{G}{c^2}\left[6(M_S + M_{BH}) + \frac{4\,M_S\,M_{BH}}{M_S + M_{BH}}\right]. \qquad (25)$$

We use this formula to estimate roughly the GR effect. In Figure 7, we draw the critical radii for the IRR sequence and the non-dimensional radius $\hat{r}_{GR}$ which is defined as follows:

Table 6. Physical quantities for stationary sequences of the IRR binary systems.

$\tilde{d}$	$\bar{d}_G$	$\bar{\Omega}$	$\bar{J}$	$\bar{E}$	$T/\|W\|$	VC	$\bar{R}$
			$M_S/M_{BH} = 1$ and $N = 0.5$				
2.2	2.856	3.449(-1)	1.223	-7.239(-1)	1.790(-1)	2.159(-2)	1.009
2.15	2.848	3.467(-1)	1.222	-7.240(-1)	1.797(-1)	2.163(-2)	1.009
2.1	2.842	3.479(-1)	1.223	-7.240(-1)	1.802(-1)	2.171(-2)	1.010
2.05	2.841	3.484(-1)	1.223	-7.239(-1)	1.805(-1)	2.184(-2)	1.010
			$M_S/M_{BH} = 1$ and $N = 1.0$				
2.3	2.804	3.507(-1)	1.194	-6.765(-1)	1.635(-1)	3.177(-3)	1.004
2.25	2.792	3.532(-1)	1.191	-6.772(-1)	1.641(-1)	3.159(-3)	1.005
2.2	2.783	3.550(-1)	1.190	-6.776(-1)	1.645(-1)	3.141(-3)	1.005
2.15	2.778	3.560(-1)	1.189	-6.780(-1)	1.648(-1)	3.108(-3)	1.005
			$M_S/M_{BH} = 0.5$ and $N = 0.5$				
2.6	2.692	3.252(-1)	2.164	-8.419(-1)	2.418(-1)	1.712(-2)	1.010
2.55	2.684	3.269(-1)	2.163	-8.424(-1)	2.426(-1)	1.715(-2)	1.011
2.5	2.678	3.282(-1)	2.162	-8.425(-1)	2.433(-1)	1.721(-2)	1.011
2.45	2.674	3.291(-1)	2.162	-8.426(-1)	2.437(-1)	1.729(-2)	1.011
2.4	2.673	3.295(-1)	2.162	-8.426(-1)	2.440(-1)	1.741(-2)	1.012
			$M_S/M_{BH} = 0.5$ and $N = 1.0$				
2.6	2.620	3.361(-1)	2.112	-8.004(-1)	2.263(-1)	1.855(-3)	1.007
2.55	2.614	3.372(-1)	2.110	-8.010(-1)	2.266(-1)	1.829(-3)	1.007
2.5	2.612	3.378(-1)	2.109	-8.012(-1)	2.267(-1)	1.774(-3)	1.008
			$M_S/M_{BH} = 0.2$ and $N = 0.5$				
3.4	2.575	3.096(-1)	4.326	-1.115	3.204(-1)	1.074(-2)	1.011
3.3	2.558	3.131(-1)	4.315	-1.117	3.219(-1)	1.068(-2)	1.012
3.2	2.544	3.159(-1)	4.308	-1.119	3.231(-1)	1.064(-2)	1.013
3.1	2.535	3.177(-1)	4.303	-1.121	3.240(-1)	1.065(-2)	1.014
3.0	2.532	3.184(-1)	4.302	-1.121	3.243(-1)	1.072(-2)	1.014
			$M_S/M_{BH} = 0.2$ and $N = 1.0$				
3.6	2.543	3.137(-1)	4.268	-1.073	3.043(-1)	1.739(-4)	1.007
3.5	2.518	3.184(-1)	4.250	-1.078	3.057(-1)	9.681(-5)	1.008
3.4	2.498	3.224(-1)	4.234	-1.083	3.069(-1)	2.461(-6)	1.009
3.3	2.483	3.254(-1)	4.222	-1.086	3.078(-1)	1.047(-4)	1.010
3.2	2.474	3.273(-1)	4.214	-1.088	3.084(-1)	2.389(-4)	1.010
			$M_S/M_{BH} = 0.1$ and $N = 0.5$				
4.0	2.493	3.106(-1)	7.037	-1.476	3.727(-1)	6.340(-3)	1.013
3.9	2.482	3.129(-1)	7.025	-1.480	3.735(-1)	6.258(-3)	1.014
3.8	2.474	3.146(-1)	7.016	-1.482	3.742(-1)	6.191(-3)	1.015
3.7	2.469	3.157(-1)	7.011	-1.483	3.746(-1)	6.145(-3)	1.015
3.65	2.467	3.160(-1)	7.009	-1.484	3.747(-1)	6.135(-3)	1.015
			$M_S/M_{BH} = 0.1$ and $N = 1.0$				
4.3	2.463	3.149(-1)	6.956	-1.441	3.589(-1)	9.621(-4)	1.009
4.2	2.445	3.183(-1)	6.933	-1.448	3.598(-1)	1.042(-3)	1.010
4.1	2.431	3.212(-1)	6.913	-1.453	3.605(-1)	1.167(-3)	1.011
4.0	2.420	3.235(-1)	6.898	-1.457	3.611(-1)	1.303(-3)	1.011
3.9	2.412	3.250(-1)	6.887	-1.460	3.614(-1)	1.489(-3)	1.012

$$\hat{r}_{GR} \simeq \frac{G\,M_S}{c^2\,R_N}\,\frac{1}{(1\,+\,M_{BH}/M_S)^{1/3}} \times \left[6\left(1+\frac{1}{M_S/M_{BH}}\right)+\frac{4}{1\,+\,M_S/M_{BH}}\right], \quad (26)$$

where the normalization is the same as equation (21). The factor GM_S/c^2R_N expresses the compactness of the neutron star. We have chosen $GM_S/c^2R_N = 1/5$, $1/8$ and $1/10$. Values of $1/5$ and $1/10$ almost correspond to those of typical neutron stars with, say, $M_S = 1.35\,M_\odot$, $R_N = 10\,\mathrm{km}$, and $M_S = 0.68\,M_\odot$, $R_N = 10\,\mathrm{km}$, respectively.

In this figure, three parallel curves drawn from upper left to lower right are those of $\hat{r}_{GR}$ and they correspond to $GM_S/c^2R_N = 1/5$, $1/8$ and $1/10$ from the top to the bottom curves, respectively. We can see that r_{GR}, which is the instability limit due to the GR effect, can be comparable with the Roche-Riemann radius r_R for a binary system with a less compact neutron star with $GM_S/c^2R_N \sim 1/8$ and moderate mass ratios. Therefore the configuration at

Figure 7. Plots of the critical radii r_{dyn} and r_R for the IRR sequences as a function of the mass ratio M_S/M_{BH}. Present results for polytropic indices $N = 0, 0.5$ and 1.0 are the same as those drawn in Figure 4(c). Three parallel curves drawn from upper left to lower right are those of $\hat{r}_{GR}$ which correspond to $GM_S/c^2R_N = 1/5$ (upper curve), 1/8 and 1/10 (lower curve).

the Roche-Riemann limit r_R could be stable even if the GR effect is included and hence the mass overflow instead of unstable plunge is expected to occur. The same mechanism can be applied for the Roche type binary systems, because, as we can see from Tables 2 and 4, the values of r_R are almost the same both for the Roche binary systems and for the IRR binary systems.

Taniguchi & Nakamura (1996) have investigated stability of the Roche type binary systems by using the improved pseudo-Newtonian potential and the ellipsoidal approximation. Because of the ellipsoidal approximation, the hydrodynamical instability limit always appears on the solution sequence of their result as LRS1, which is in contrast to our present result. Recently, Kluźniak & Lee (1997) performed numerical simulations for binary systems of a point source and a synchronous rotating star by using the SPH method. They reported models with mass ratios $M_S/M_{BH} = 1$ and 0.31 for polytropes with $N = 0.5$. In their paper, they have shown that not the unstable plunge but the mass transfer occurs for $M_S/M_{BH} < 0.8$. The resulting mass transfer from NS to BH and matter distribution around the BH vary significantly. They have concluded that the system is a promising source of GRB. Our computation qualitatively agrees with their result. For the Roche binary with $N = 0.5$, our result shows that r_{sec} disappears around $M_S/M_{BH} \lesssim 0.2$. Although this value is different from the result of simulations, values of radii r_{sec} and r_R, and hence r_{dyn} are very close as seen in Figure 2(d). Therefore the possibility of mass overflow is also supported in this respect.

If such a mass overflow occurs, we need to consider the following problem. Does this mass transfer continue stably or not? Stable mass transfers lead to the survival of a less massive NS and the BH–NS binary systems with a much smaller mass ratio M_S/M_{BH} are formed after the mass transfer. This process depends on several factors such as the amount of mass escaped from the NS and that accreted onto the BH, and on how the structure of NS and its Roche lobe have changed as a result of overflow and so on. Qualitative discussions (see Kochanek 1992 ; Bildsten & Cutler 1992, and references therein) suggest that such stable mass transfer seems difficult. Quantitative examination is possible by using our stationary method. We will investigate this problem in the future.

4.2 GW signal at the Roche(–Riemann) limit

Let us consider the case that the BH–NS binary evolves stably along the stationary sequence and reach the Roche(-Riemann) limit r_R without suffering from hydrodynamical instability. It is natural to expect that the GW signal emitted from such a binary system would change at a critical radius and from the frequency there we may be able to determine the critical radius, r_R in our case.

By comparing Tables 2 and 4, the physical quantities around the critical radii are almost the same for the Roche and the IRR type binary systems. In particular, the difference of r_R between the Roche and the IRR types is less than $2, 1$ and 0.5% for polytropes with $N = 0, 0.5$ and 1, respectively. This is irrespective of the mass ratio for the range $0.1 \lesssim M_S/M_{BH} \lesssim 1$. Therefore, we cannot decide whether the star is in a synchronously rotating state or in an irrotational state from the observation of the GW. In other words, the GW signal contains information about EOS but not about the rotational state. Therefore we can only determine r_R and the stiffness of the NS. On the other hand, it seems difficult to extract some new information for the viscosity of neutron matter from the GW signal emitted at this stage. Note, however, the spin of NS may be accurately determined by using the higher order PN expansion for the inspiraling phase (see for e.g. Mino et. al. 1997, and references therein).

4.3 Conclusions

In this paper we have systematically examined the sequences of a point source and a fluid star binary systems. We have assumed the fluid star to be a polytrope and employed Newtonian gravity. We have found that the critical radii, r_{dyn}, r_{sec} and r_R are quantitatively different from those computed by using the ellipsoidal approximation for the star. We have clarified that r_{dyn} or r_{sec} disappears even on binary sequences with a moderate mass ratio and a stiff EOS and hence the existence of dynamically stable Roche(-Riemann) limit has been shown. This suggests a possibility of mass overflow instead of an unstable plunge due to the hydrodynamical instability of binary systems at the final stage of the binary evolution due to the GW emission.

For further investigations, we should take into account effects of the black hole field, the radial velocity and so on. Though it is very difficult to numerically construct the realistic BH, the pseudo-Newtonian potential can represent the marginal instability of the GR effect around the Schwarzschild BH field. Taniguchi & Nakamura (1996) have used an improved pseudo-Newtonian potential and the ellipsoidal approximation to determine the innermost stable circular orbit of BH-NS systems. Such a pseudo-Newtonian potential will be included straightforwardly in our present scheme for a fully deformed configuration of stars.

Newtonian approximation for the fluid star component is insufficient for NS models whose gravity is considered as strong as, more or less, the second post-Newtonian approximation of general relativity. Recently several authors have

solved the NS-NS configuration including the GR effect (Shibata 1997 ; Baumgarte et al. 1997). The formulation for the irrotational star in GR gravity is also proposed (Bonazzola, Gourgoulhon & Marck 1997 ; Asada 1998 ; Shibata 1998 ; Teukolsky 1998). By implementing these results, the GR effect could be included step by step, and finally it will be possible to construct the quasi-stationary evolution of the BH–NS systems.

ACKNOWLEDGMENTS

We would like to thank Prof. J. C. Miller for carefully reading the manuscript and for helpful comments. KU would also like to thank Prof. D. W. Sciama and Dr. A. Lanza for their warm hospitality at ICTP and SISSA. Numerical computations were carried out by at the Astronomical Data Analysis Center of the National Astronomical Observatory, Japan.

REFERENCES

Abramovici A. et al., 1992, Science, 256, 325
Aizenman M. L., 1968, ApJ, 153, 511
Asada H., 1998, Phys. Rev. D, in press, (gr-qc/9804003)
Baumgarte T. W., Cook G. B., Scheel M. A., Shapiro S. L., Teukolsky S. A., 1997, Phys. Rev. D, submitted, (gr-qc/9709026)
Bildsten L., Cutler C., 1992, ApJ, 400, 175
Bonazzola S., Gourgoulhon E., Marck J.-A., 1997, Phys. Rev. D, in press (gr-qc/9710031)
Chandrasekhar S., 1969, Ellipsoidal Figures of Equilibrium, Yale University Press, New Haven
Cutler C. et al., 1993, Phys. Rev. Lett., 70, 2984
Eriguchi Y., Futamase T., Hachisu I., 1990, A&A, 231, 61
Hachisu I., 1986, ApJS, 62, 461
Hachisu I., Eriguchi Y., 1984a, Publ. Astron. Soc. Japan, 36, 239
Hachisu I., Eriguchi Y., 1984b, Publ. Astron. Soc. Japan, 36, 259
Kidder L. E., Will C. M., Wiseman A. G., 1992, Class. Quantum Gravity, 9, L125
Kluźniak W., Lee W. H., 1997, ApJ, 494, L53
Kochanek C. S., 1992, ApJ, 398, 234
Lai D., Rasio F. A., Shapiro S. L., 1993a, ApJ, 406, L63
Lai D., Rasio F. A., Shapiro S. L., 1993b, ApJS, 88, 205, LRS1
Lai D., Rasio F. A., Shapiro S. L., 1994a, ApJ, 420, 811, LRS2
Lai D., Rasio F. A., Shapiro S. L., 1994b, ApJ, 423, 344
Miller B.D., 1974, ApJ, 187, 609
Mino Y., Sasaki M., Shibata M., Tagoshi H., Tanaka T., 1997, Prog. Theor. Phys. Suppl., 1, 183
Misner C. W., Thorne K. S., Wheeler J. A., 1970, Gravitation, W. H. Freeman and Company, San Francisco
New K. C. B., Tohline J. E., 1997, ApJ, 490, 311
Oohara K., Nakamura. T., Shibata M., 1997, Prog. Theor. Phys. Suppl., 128, 183
Ostriker J. P., Mark J. W-K., 1968, ApJ, 151, 1075
Paczyński B., 1991, Acta Astron., 41, 257
Rasio F. A., Shapiro S. L., 1992, ApJ, 401, 226
Rasio F. A., Shapiro S. L., 1994, ApJ, 432, 242
Ruffert M., Rampp M., Janka H.-T., 1997, A&A , 321, 991
Shapiro S. L., Teukolsky S. A., 1983, Black Holes, White Dwarfs and Neutron Stars, Wiley, New York
Shibata M., 1997, Phys. Rev. D, 55, 6019
Shibata M., 1998, Phys. Rev. D, submitted, (gr-qc/9803085)
Shibata M., Oohara K., Nakamura. T., 1997, Prog. Theor. Phys., 98, 1081
Taniguchi K., Nakamura T., 1996, Prog. Theor. Phys., 96, 693
Tassoul J.-L., 1978, Theory of Rotating Stars, Princeton Univ. Press, Princeton
Teukolsky S. A., 1998, ApJ, submitted, (gr-qc/9803082)
Uryū K., Eriguchi Y., 1996, MNRAS, 282, 653
Uryū K., Eriguchi Y., 1998a, ApJS, in press, Paper I
Uryū K., Eriguchi Y., 1998b, MNRAS, 296, L1, (astro-ph/9712203)
Uryū K., Eriguchi Y., 1998c, MNRAS, in press

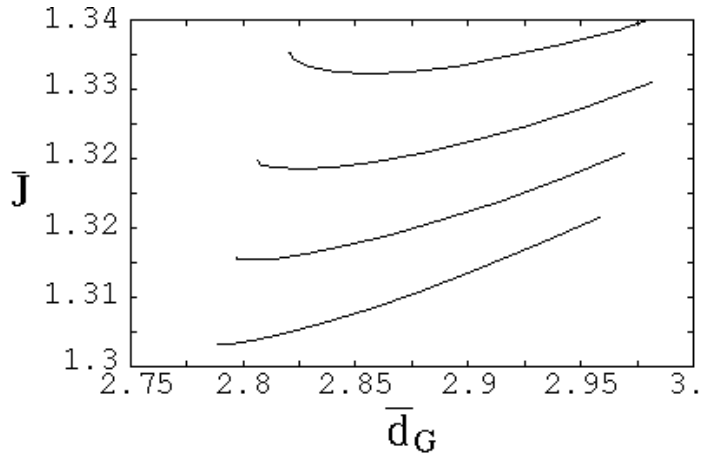

Figure 1 (a)

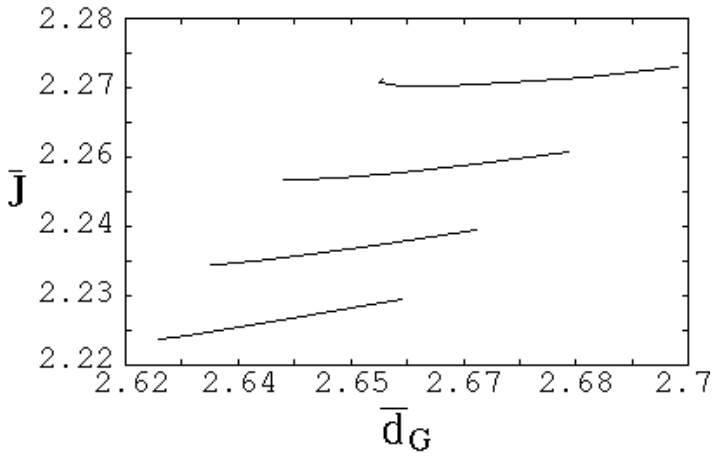

Figure 1 (b)

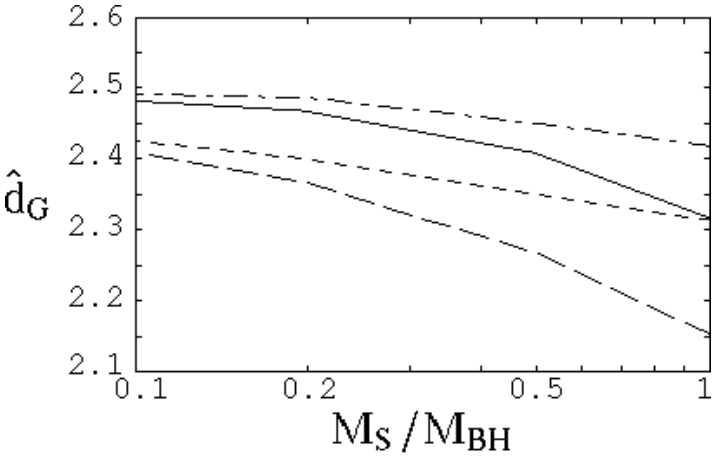

Figure 2 (a)

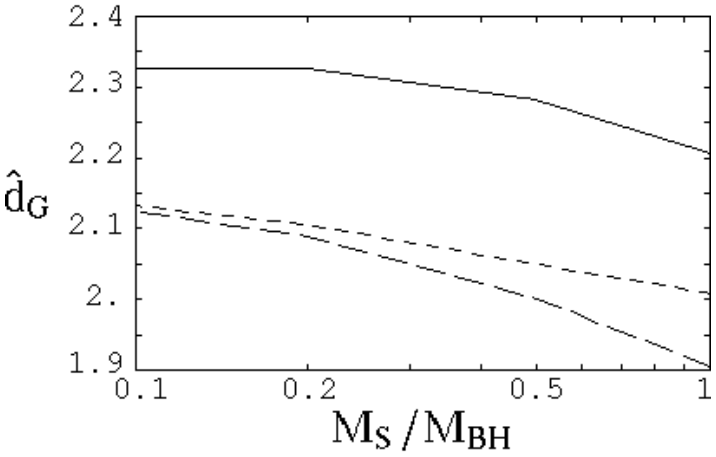

Figure 2 (b)

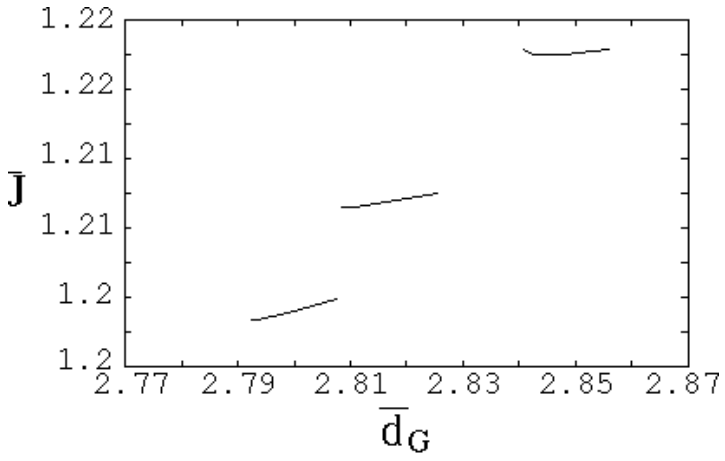

figure 3 (a)

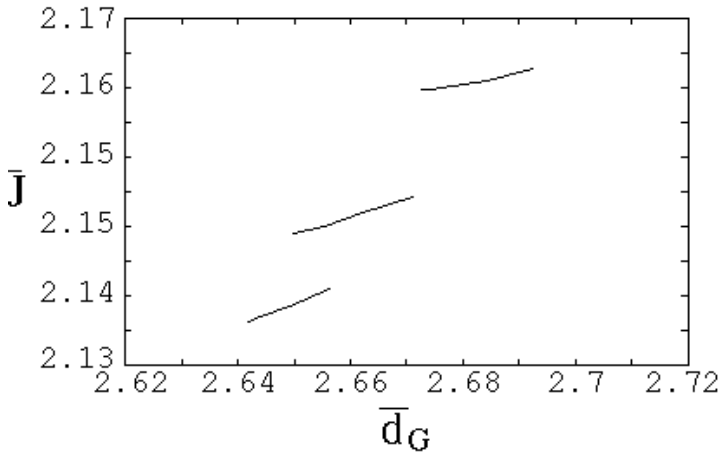

figure 3 (b)

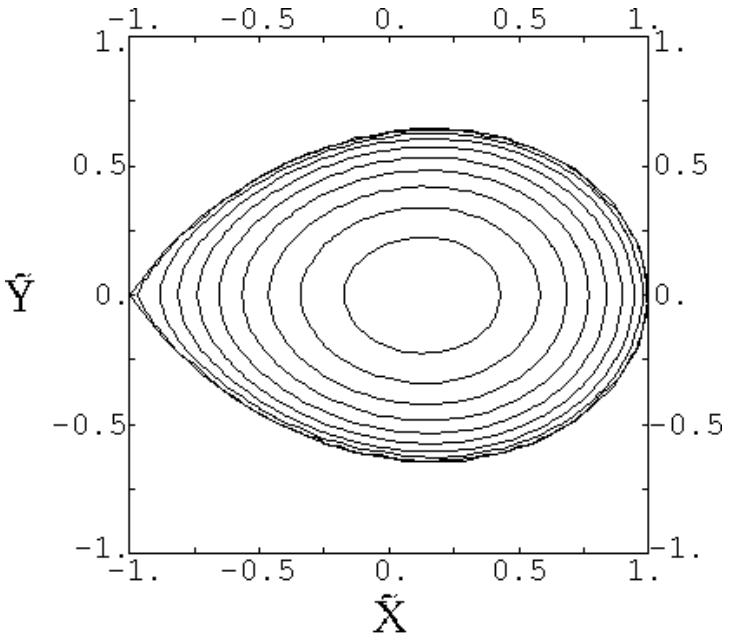

Figure 5 (a)

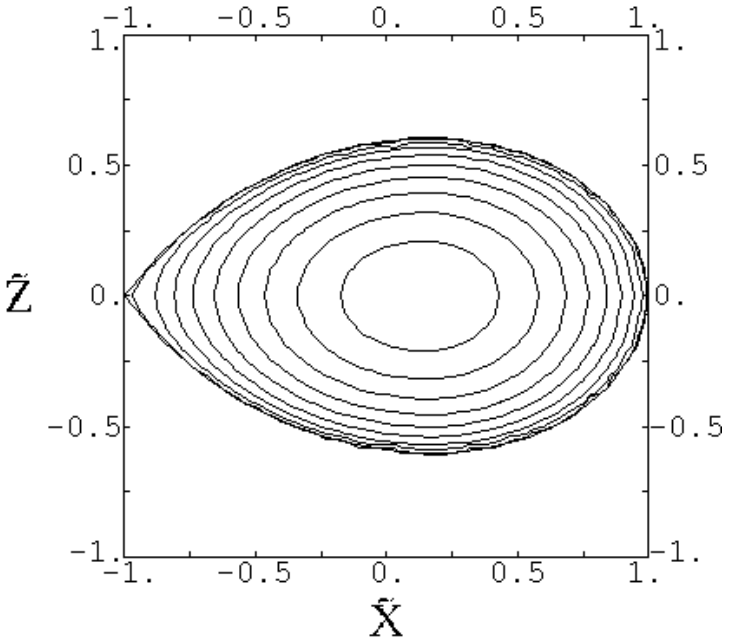

Figure 5 (b)

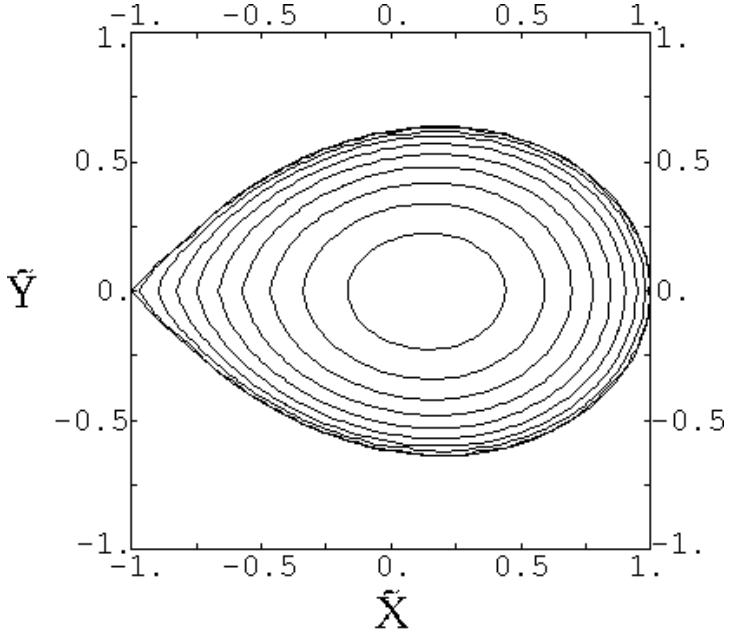

figure 6 (a)

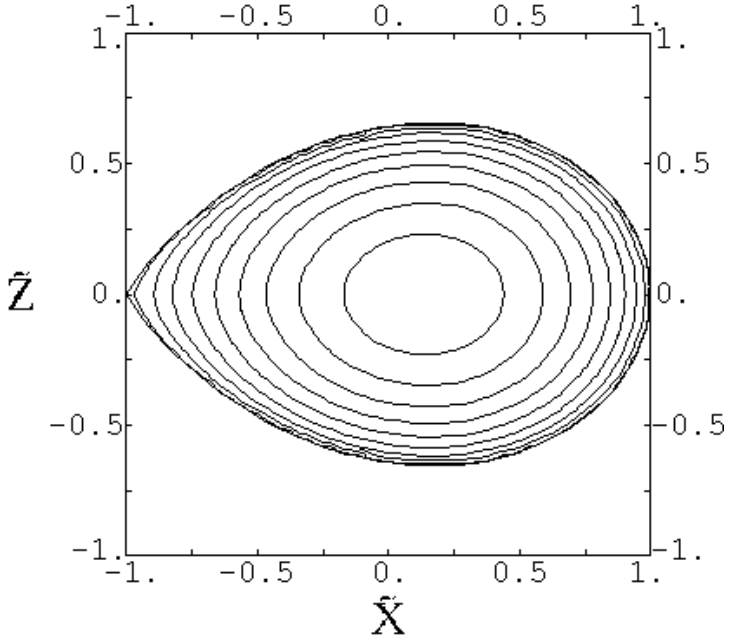

figure 6 (b)

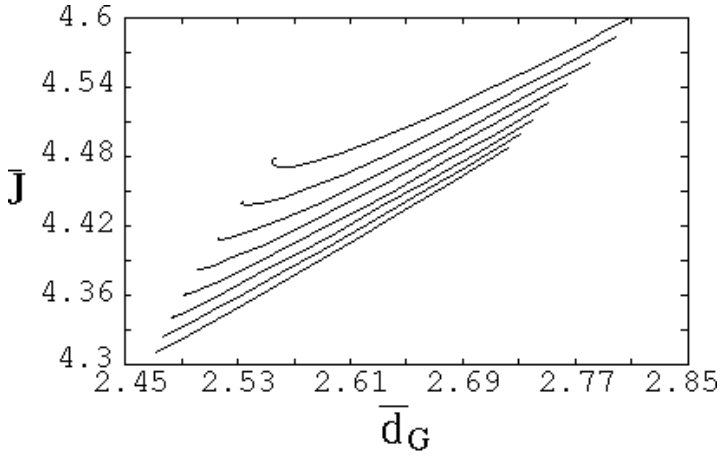

Figure 1 (c)

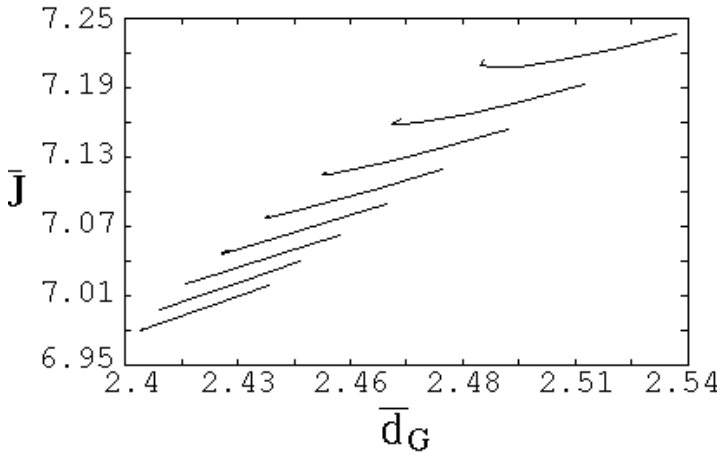

Figure 1 (d)

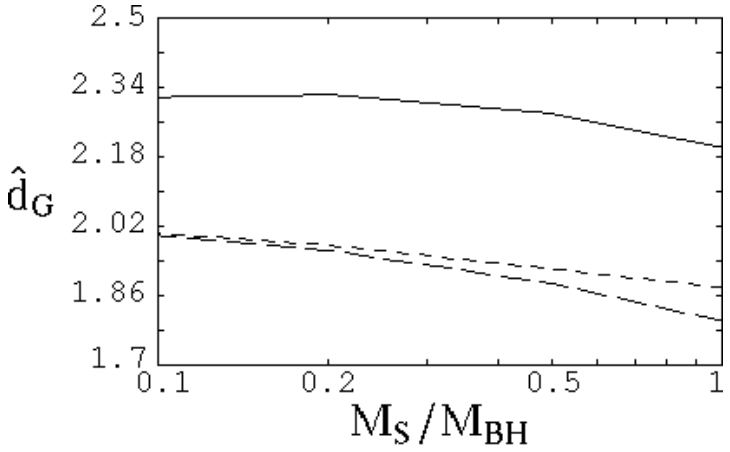

Figure 2 (c)

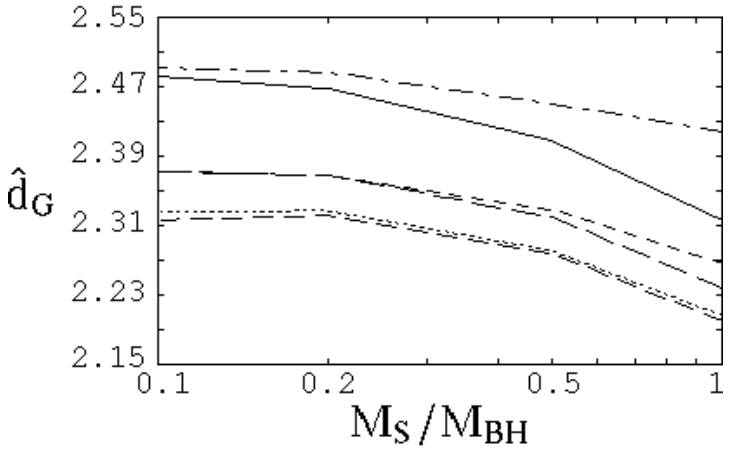

Figure 2 (d)

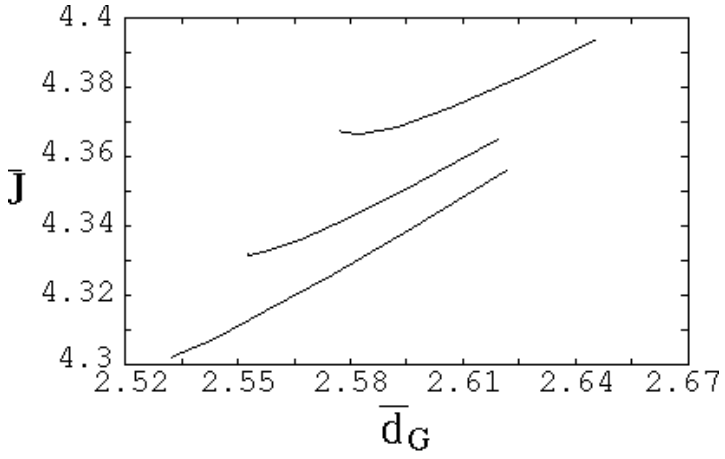

figure 3 (c)

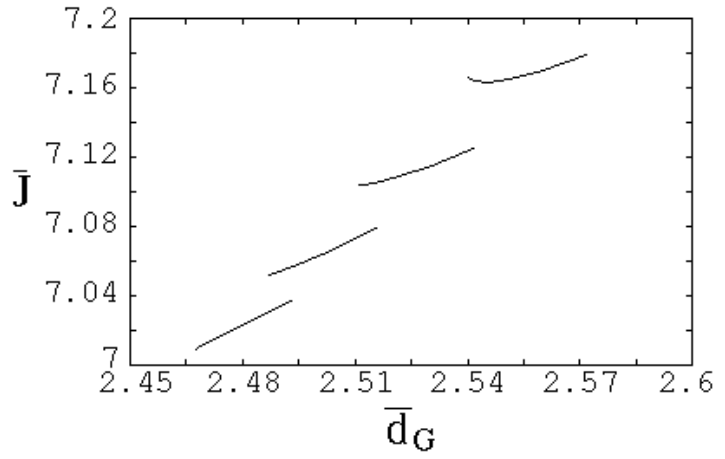

figure 3 (d)

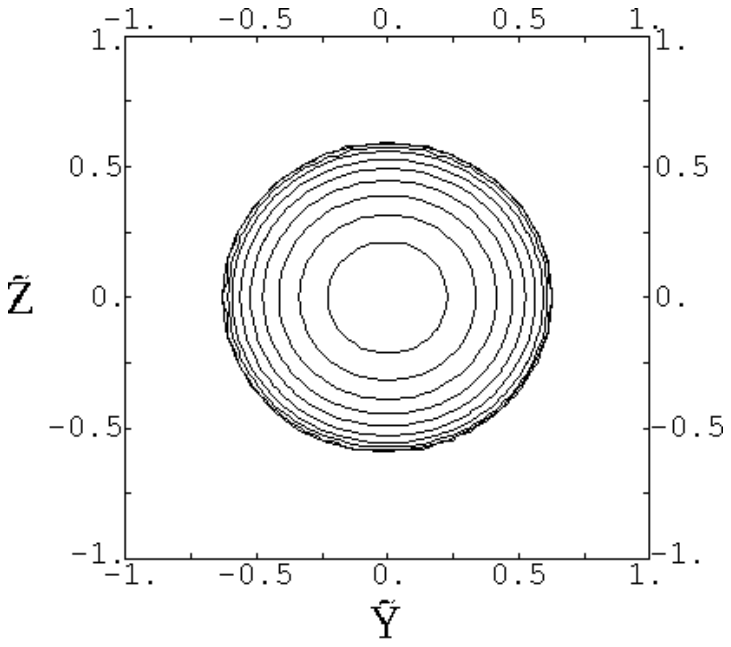

Figure 5 (c)

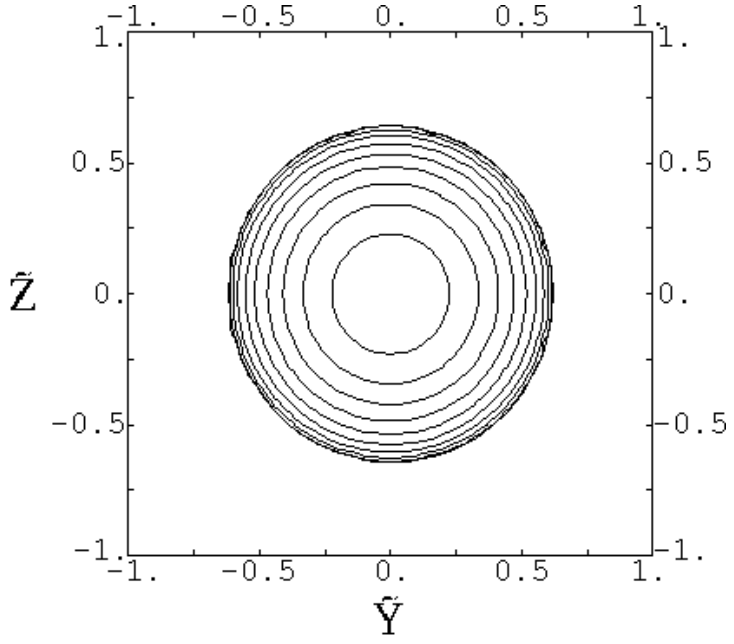

figure 6 (c)

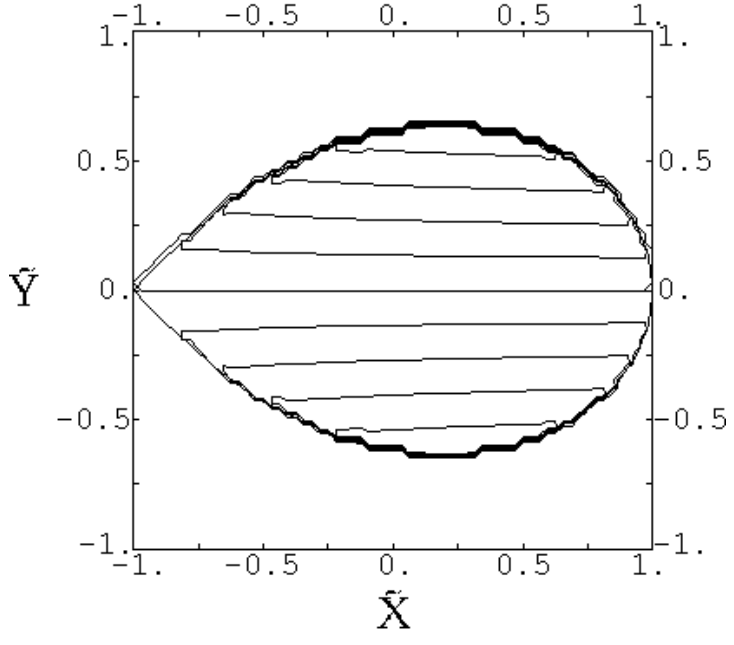

figure 6 (d)

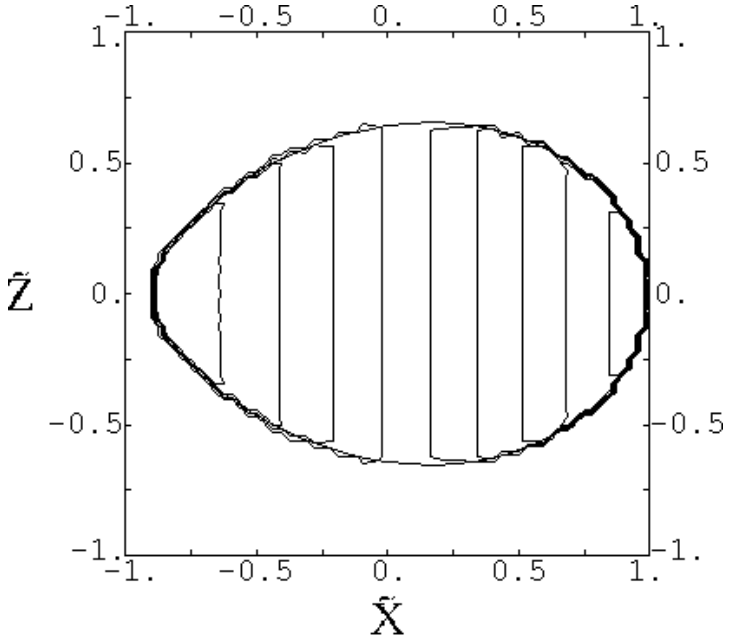

figure 6 (e)

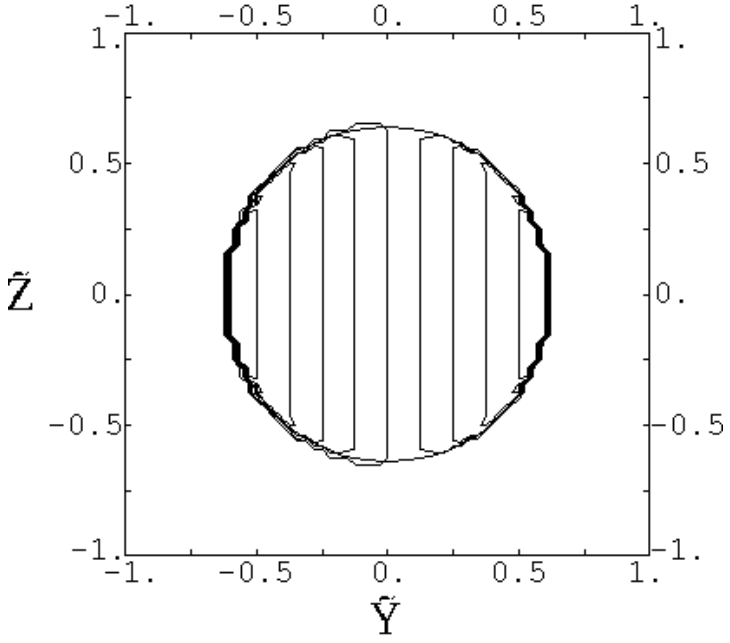

figure 6 (f)

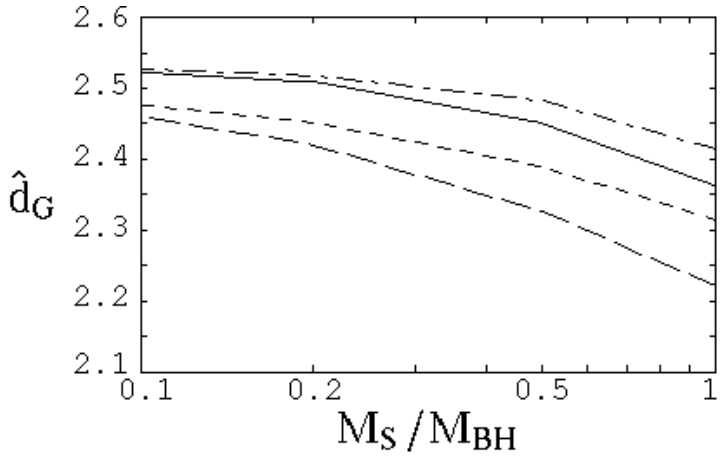

figure 4 (a)

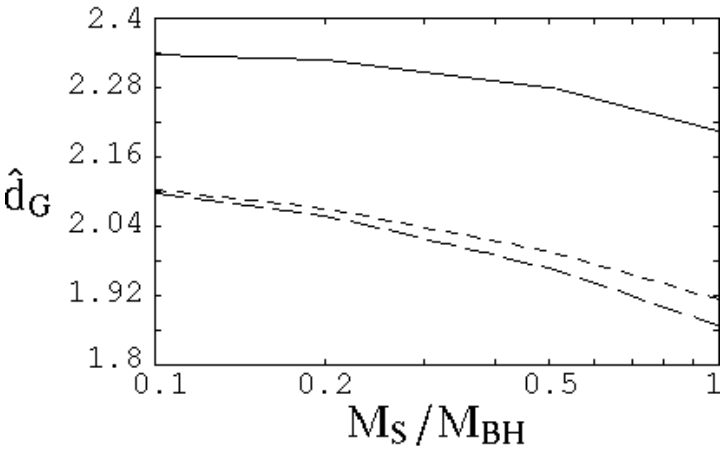

figure 4 (b)

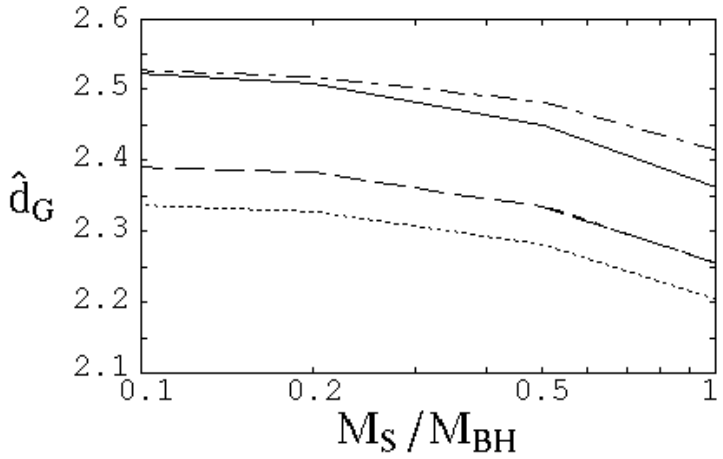

figure 4 (c)

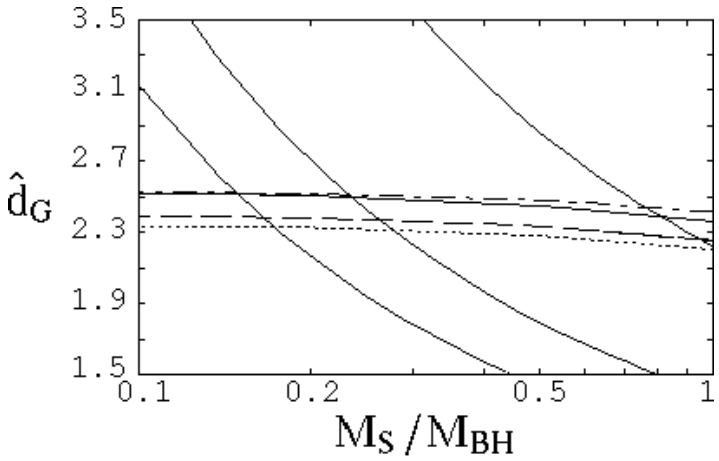

Figure 7